Comparative study of thickness dependence of critical current density of $YBa_2Cu_3O_{7-\delta}$ on (100) $SrTiO_3$ and on rolling-assisted biaxially textured substrates

B.W. Kang, A. Goyal,[a] D.F. Lee, J.E. Mathis,[b] E.D. Specht, P.M. Martin, and D.M. Kroeger
Metals and Ceramics Division, Oak Ridge National Laboratory, Oak Ridge, Tennessee, 37831

M. Paranthaman and S. Sathyamurthy
Chemical and Analytical Sciences Division, Oak Ridge National Laboratory, Oak Ridge, Tennessee 37831

(Received 6 June 2001; accepted 19 April 2002)

We investigated the dependence of critical current density (J_c) on thickness of $YBa_2Cu_3O_{7-\delta}$ (YBCO) films grown by pulsed laser deposition on (100) $SrTiO_3$ (STO) and on rolling-assisted biaxially textured substrates (RABiTS). The thickness of YBCO films varied from 0.19 to 3 μm. The highest J_cs of 5.3 and 2.6 MA/cm^2 at 77 K, self-field were obtained for 0.19-μm YBCO films on STO and RABiTS, respectively. J_c was found to decrease exponentially with YBCO thickness on both substrates. However, the results suggest different mechanisms are responsible for the J_c reduction in the two cases. On STO, growth of *a*-axis grains within *c*-axis films and broadening of the in-plane texture were observed in thick films. On RABiTS, degradation in cube texture as well as development of a porous surface morphology were found to correlate with film thickness.

I. INTRODUCTION

Significant progress has been made toward fabrication of second-generation high temperature superconducting (HTS) coated conductors using the $YBa_2Cu_3O_{7-\delta}$ (YBCO) compound. The main goal is to utilize the strong pinning properties of YBCO in magnetic fields at liquid nitrogen temperature, which are usually required for electric power applications including motors, generators, magnets, and power transmission lines. Since YBCO coatings on short metal substrates were demonstrated to have critical current density (J_c) values over 1 MA/cm^2 at 77 K,[1–4] great efforts have been devoted to achieve such performance over meter-long lengths. In addition to scaling up to long lengths, parallel attention is focused on improving the critical current (I_c) of such tapes. Increasing the current-carrying capacity will increase the engineering critical current density (J_E; overall J_c), which is determined by the total thickness of the YBCO coating and substrate and reduces the manufacturing cost per unit performance.

The simplest way to increase I_c of a conductor is to increase the thickness of YBCO coatings. However, it has been reported that the J_c decreases rapidly as the thickness of epitaxial YBCO films increases on both single-crystal substrates[5–11] and on metal substrates.[12,13] While the trend of an exponential drop of J_c with YBCO thickness seems to be universal regardless of the deposition technique, the cause of this drop is not yet clear. In the literature, a transition to *a*-axis orientation,[5,6,8] a loss of in-plane and/or out-of-plane texture,[7,9] a decrease in the number of pinning sites,[10] and a change in the microstructure[12] have been reported as possible causes for the J_c drop. Real applications of HTS require wires to carry large currents. Hence it is important to determine whether thick YBCO films with good transport properties can be made on textured metal substrates. In this paper we report a comparative study of the thickness dependence of J_c of YBCO grown by pulsed laser deposition (PLD) on (100) $SrTiO_3$ (STO) single crystal substrates and on rolling-assisted biaxially textured substrates (RABiTS). From the investigation of structural and superconducting properties of a series of YBCO films, possible mechanisms for J_c reduction on both substrates are discussed.

II. EXPERIMENTAL

The preparation of RABiTS (Ni plus buffer layers unit) has been described in detail elsewhere.[2,13–16] Biaxially textured Ni substrates were obtained from

[a]e-mail: goyala@ornl.gov
[b]Present address: Physical Science Department, Embry-Riddle Aeronautical University, Daytona Beach, Florida 32114

high-purity (99.99%) Ni bars containing randomly oriented grains. The bars were first mechanically deformed by cold-rolling and then annealed in vacuum at 1000–1100 °C for 1 h to obtain the desired {100}⟨100⟩ cube texture. An epitaxial layer of CeC_2, approximately 12 nm thick, was deposited by electron beam evaporation of cerium metal onto Ni at 650 °C. Oxidation of Ni during the heat-up phase was prevented by the introduction of a reducing forming gas (96% Ar + 4% H_2). The cerium oxide was formed by the *in situ* reaction of the cerium with water vapor (1×10^{-5} torr) supplied to the vacuum system during deposition.[17,18] The deposition of CeO_2 was followed by the deposition of a 300-nm-thick layer of yttria-stabilized zirconium oxide (YSZ) and 20-nm-thick CeO_2 cap layer by radio-frequency (rf) sputtering while the substrate temperature was maintained at 780 °C in 1×10^{-2} torr of forming gas and 2×10^{-6} torr of water vapor.

Both the oxide-buffered and STO substrates were then silver pasted onto the heater in the PLD chamber. The dimensions of STO and RABiTS were 3 mm × 1.5 cm × 0.5 mm and 3 mm × 2.5 cm × 50 μm, respectively. An excimer laser (LPX 305i, Lambda Physik AG, Göttinger, Germany), operating at a wavelength of 308 nm, was focused on the YBCO target to produce approximately 4 J/cm^2 fluence. During the deposition, the substrates were kept at 790 °C within an atmosphere of 120 mtorr O_2. To minimize both the rate of cone formation and changes in stoichiometry on the surface of the YBCO target during laser irradiation, the YBCO target was rotated at 21 revolutions per minute. After the deposition was completed, the samples were cooled to room temperature at the rate of 5 °C/min, while the O_2 pressure was increased to 550 torr to ensure full oxygen uptake by the YBCO films. The YBCO growth rate was approximately 0.5–1 nm/s; film thickness was varied from 0.19 to 3 μm by changing the deposition time. The thickness of each sample was determined by both Rutherford backscattering spectroscopy (RBS) and alpha step profilometer scans. A standard four-contact configuration was used to evaluate electrical properties of the samples. Values of J_c were determined by a 1 μV/cm criterion. The crystal structure and the texture of the selected films were characterized by a Huber high-resolution x-ray diffractometer (XRD) and a four-circle diffractometer (Picker Corp., Cleveland, OH), respectively. Pole figures were also collected for selected samples to determine the percentage of cube texture. Microstructural analyses were conducted by using a field emission scanning electron microscope (SEM; S-4100, Hitachi Ltd., Tokyo, Japan).

III. RESULTS AND DISCUSSION

In Fig. 1, the critical current density (J_c) is plotted as a function of YBCO thickness on the RABiTS. Also shown for comparison are the J_c values on (100) STO. As

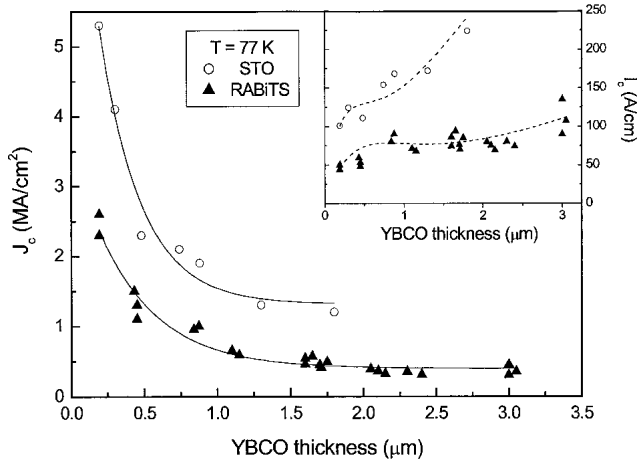

FIG. 1. Critical current density as a function of YBCO film thickness on RABiTS and on STO (100) substrates. Solid lines are an empirical fit of exponential decay function. Inset shows the calculated critical current (I_c) for a 1 cm width as a function of film thickness on both substrates. Dashed lines are calculated I_c from the empirical fits of J_c.

expected, the highest J_cs of 5.3 and 2.6 MA/cm^2 at 77 K, self-field were obtained for the thinnest films (0.19 μm) both on STO and on RABiTS, respectively, and J_c values decreased exponentially as YBCO thickness increased. The thickness dependence of J_c can be fit with the form $J_c = J_0 + \beta e^{-\alpha t}$, where t is the film thickness, shown as solid lines, on both substrates. From the empirical fits J_0, β, and the decay constant α were determined to be, respectively, 1.3 MA/cm^2, 7.8 MA/cm^2, and 3.8 μm^{-1} for STO, and 0.4 MA/cm^2, 3.2 MA/cm^2, and 1.8 μm^{-1} for RABiTS. In the inset of Fig. 1, the calculated critical currents (I_c) for 1-cm-wide sample are plotted as a function of YBCO thickness for both substrates. Within the thickness region we investigated (up to 3 μm), I_c increases with film thickness for both substrates, however the rate of increase for RABiTS is much lower than that for STO. Also shown as dotted lines are calculated I_cs from the empirical fitting function of J_c for comparison. No evidence was seen for a decline in I_c very thick films as was reported in Ref. 12.

Even though J_c and I_c have similar thickness dependencies on the two substrates, the mechanisms of J_c drop in thick samples seem to be different. Although an appearance of a-axis-oriented ($a_\perp$) material can be observed on both substrates as YBCO thickness increases, the fraction of $a_\perp$ material is much smaller on RABiTS compared to that on STO. Since STO (l00) peaks overlap with YBCO (00l) in θ-2θ scans, both XRD χ-scans and θ-2θ scans were performed for films on STO to quantify the fraction of $a_\perp$ material. For films on RABiTS, θ-2θ scans provided a good estimate of the percentage of $a_\perp$ grains.

Figure 2(a) shows the χ-scan of the 1.8-μm-thick YBCO film on STO, and Fig. 2(b) the θ-2θ scan of the 3-μm-thick YBCO on RABiTS. To calculate the amount

of $a_\perp$ versus c-axis-oriented ($c_\perp$) material in the YBCO film from the XRD χ-scans and the XRD θ-2θ scans, x-ray absorption effects also need to be considered, since it is possible that $a_\perp$ grains lie primarily at the top surface of the film and hence diffract more strongly. To simplify the picture, we consider the case when all the $a_\perp$ grains are sitting at the top surface of the film. We assume that the $a_\perp$ material forms a layer of thickness, t_a on top of a layer of $c_\perp$ material of thickness t_c (Fig. 3). Such a case has been reported previously for a 5-μm-thick epitaxial YBCO film on MgO.[7] Using this simple model, the ratio of $a_\perp$ to $c_\perp$ material can be found from measured x-ray intensities I_a and I_c using a simple calculation. Taking $i_a/i_c = 1.0$ to be the peak intensity ratio for a random powder, $L = 9.1$ μm to be the x-ray penetration depth for Cu K_α into YBCO, and θ to be the Bragg angle, we have

$$\frac{I_a}{I_c} = \frac{i_a}{i_c} \frac{\int_0^{t_a} \exp[-2z/(L\sin\theta_a)]\mathrm{d}z}{\exp[-2t_a/(L\sin\theta_c)] \int_0^{t_c} \exp[-2z/(L\sin\theta_c)]\mathrm{d}z} \approx \frac{\exp(0.56 t_a/\mu m) - 1}{1 - \exp(-0.56 t_c/\mu m)} \quad . \tag{1}$$

The calculated ratio of $a_\perp$ to $c_\perp$ material (t_a/t_c) according to formula (1) for STO and for RABiTS are listed in Tables I and II, respectively. The ratio t_a/t_c provides a lower bound for the percentage of $a_\perp$ material while the ratio I_a/I_c provides an upper bound to the percentage of $a_\perp$ material (since in this case no preferential segregation of $a_\perp$ grains on the surface of the films is assumed). For YBCO films on STO, both I_a/I_c and hence t_a/t_c increase

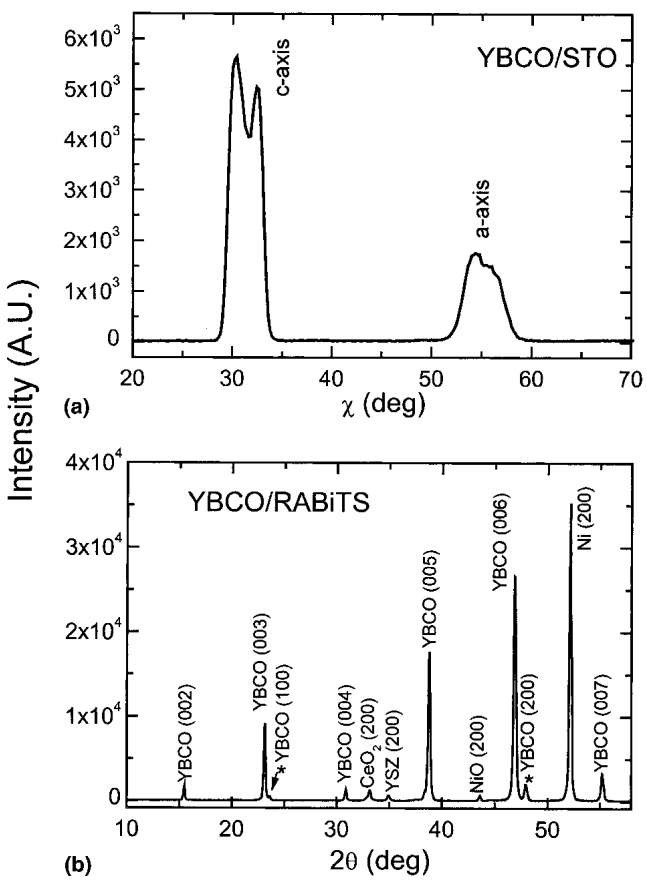

FIG. 2. (a) X-ray χ-scan for 1.8-μm-thick YBCO on STO. A significant amount of a-axis orientation is detected. (b) X-ray θ-2θ spectrum for a 3-μm-thick YBCO sample on RABiTS. Note the presence of YBCO (200) peak indicated by (*).

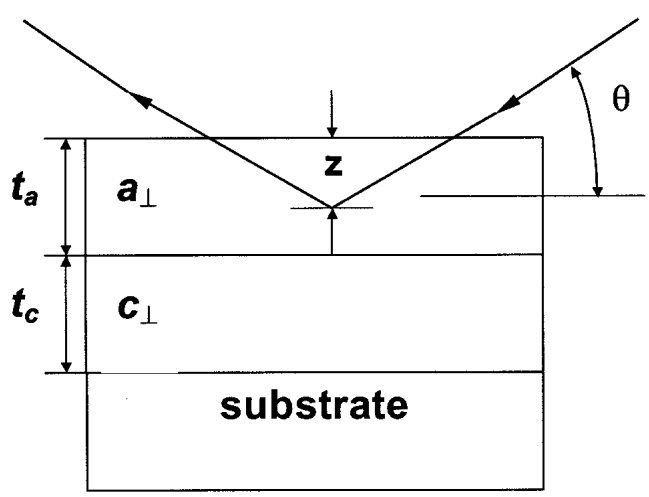

FIG. 3. Geometry used to calculate the ratio of $a_\perp$ to $c_\perp$ material.

TABLE I. Texture analysis data of a series of YBCO films with different thickness on STO.

Sample	Thickness (μm)	J_c (MA/cm^2)	I_a/I_c	t_a (μm)	t_c (μm)	t_a/t_c	In-plane texture (°)[a]	Out-of-plane texture (°)[b]
BWK-82B	0.19	5.3	0	0	0	0	1.3	0.54
BWK-115A	0.3	4.1	0	0	0	0	1.4	0.53
BWK-70C	0.44	2.1	0	0	0	0	1.3	0.6
BWK-71C	0.88	1.9	0.3	0.14	0.74	0.2	1.5	0.7
BWK-101B	1.3	1.4	0.49	0.3	1.0	0.3	2.1	0.58
BWK-100B	1.8	1.3	0.51	0.4	1.4	0.3	2.6	0.55

[a]In-plane texture is the FWHM of YBCO (103).
[b]Out-of-plane texture is the FWHM of YBCO (005).

quickly as YBCO thickness increases. For the 1.8-μm-thick film, the lower and upper bound for the percentage of $a_\perp$ grains in the film are 30% and 51%, respectively. Since J_c for $a_\perp$ films is only 2–3% of that for the $c_\perp$ films,[19,20] this essentially amounts to a J_c reduction of 30% to 50%. Hence a transition to $a_\perp$ growth is a dominant factor for the J_c decrease of YBCO films on STO. In contrast, for films on RABiTS, I_a/I_c and t_a/I_c are only

TABLE II. Texture analysis data of a series of YBCO films with different thickness on RABiTS.

Sample	Thickness (μm)	J_c (MA/cm^2)	I_a/I_c	t_a (μm)	t_c (μm)	t_a/t_c	In-plane texture[a]	Out-of-plane texture[b]	Percent cube[c]
BWK-53C	0.19	2.6	0	0	0	0	1.07	0.73	98.8
BWK-70B	0.43	1.4	0	0	0	0	1.04	0.7	90.4
BWK-73B	0.84	1.2	0.06	0.03	0.81	0.04	1.17	0.66	90.4
BWK-96B	1.2	0.54	0.03	0.02	1.18	0.02	1.07	0.73	90.5
BWK-88A	1.6	0.59	0.05	0.05	1.55	0.03	1.03	0.76	89.7
BWK-93A	3.0	0.45	0.07	0.14	2.86	0.05	1.08	0.73	79.9

[a]In-plane texture is the FWHM ratio of YBCO (103)/Ni (111).
[b]Out-of-plane texture is the FWHM ratio of YBCO (005)/Ni (200).
[c]Percent cube is calculated from YBCO (113) pole figure.

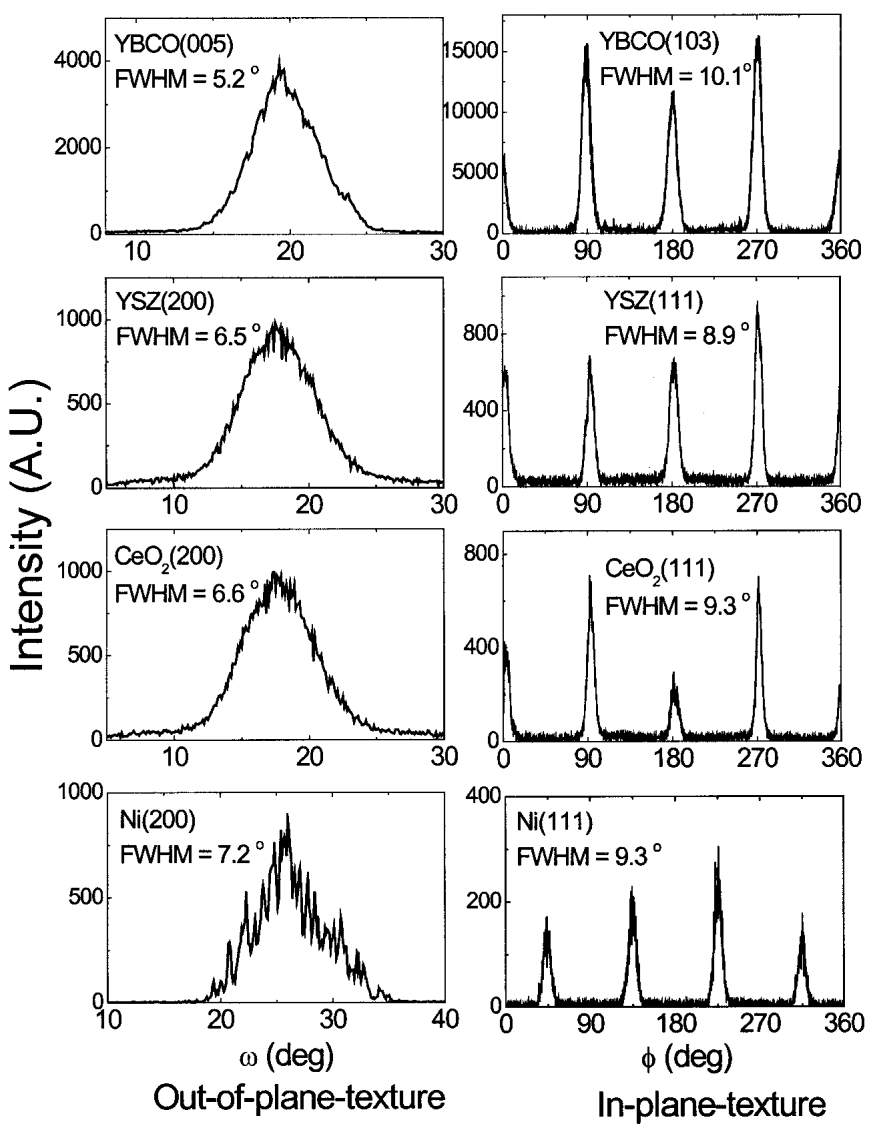

FIG. 4. The ω and ϕ scans for a 3-μm-thick YBCO film on CeO_2/YSZ/CeO_2/Ni substrate.

0.07 and 0.05, respectively, even for a 3-μm-thick YBCO. Hence growth of $a_\perp$ grains can account for only a small part of the drop of J_c in thicker films on RABiTS.

For the out-of-plane and in-plane texture analysis, XRD ω-rocking curves and ϕ-scans were performed on both substrates. For YBCO films on STO, a very sharp out-of-plane texture was maintained up to 1.8 μm, however, a significant broadening in the in-plane texture was observed in thicker films. The results of the texture measurements on STO are summarized in Table I. Interestingly, for YBCO films on RABiTS, essentially no degradation of the in-plane or out-of-plane textures is observed even for YBCO thickness up to 3 μm. Figure 4 shows the out-of-plane and the in-plane textures for a 3-μm-thick YBCO film on the standard CeO_2/YSZ/CeO_2/Ni architecture used in this study. Since the top CeO_2 and the bottom CeO_2 layers cannot be distinguished by XRD, only 4 layers are shown. It can be seen from the ω-rocking curve scan that the out-of-plane texture for the 3-μm-thick YBCO sample is still sharp. The improvement in full width at half-maximum (FWHM) of YBCO with respect to Ni substrates is commonly observed in most of YBCO samples on RABiTS, and is probably due to planar alignment with smoother surface, a gradual decrease in lattice mismatch among consecutive layers, and/or smaller grain size. This high degree of out-of-plane texture is especially important to achieve high-J_c values. The FWHM of the ϕ-scans for (103) YBCO, (111) CeO_2, (111) YSZ, and (111) Ni are 10.1°, 8.9°, 9.3°, and 9.3°, respectively, indicating that the top YBCO layer closely replicates the in-plane texture of Ni substrates. The results of the texture measurements on STO and on RABiTS are summarized in Tables I and II, respectively. Note that biaxially textured Ni substrates generally have slightly different out-of-plane and in-plane textures depending on the specific rolling and crystallization conditions [The FWHM of (111) Ni and (200) Ni used in this experiment ranges from 8° to 10°]. To make a direct and more quantitative comparison between the YBCO thickness and the crystalline quality of the films, the FWHM ratios relative to the underlying Ni are listed. No significant degradation in the out-of-plane and in-plane textures is observed with an increase in the YBCO thickness, suggesting that the change in texture is not a key mechanism contributing to the J_c drop for YBCO films on RABiTS.

Since the appearance of $a_\perp$ material and degradation of the in-plane/out-of-plane texture do not seem to have a major contribution to the reduction in J_c for YBCO films on RABiTS, it is of interest to explore possible mechanisms. Accordingly, another possible mechanism, the degree of cube texture in the YBCO films, was examined. Quantitative measurements of the cube texture were made for all the YBCO films on RABiTS. Figures 5(a)–5(d) show (113) YBCO pole figures for 0.19-, 0.45-, 1.6-, and 3.0-μm-thick films in logarithmic scale. A systematic degradation in the quality of the cube texture with increasing YBCO thickness was found. The

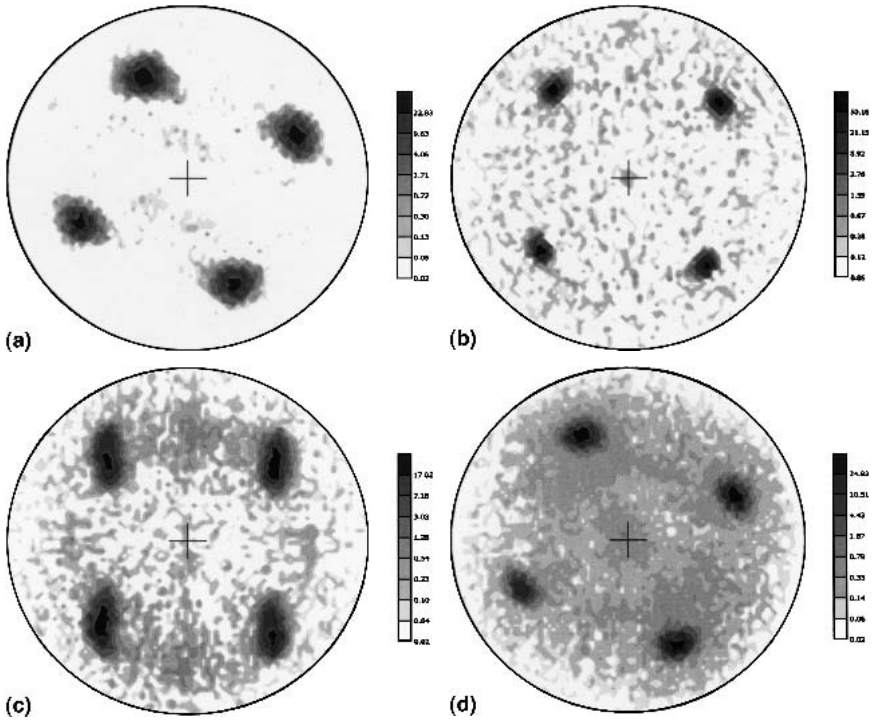

FIG. 5. (113) X-ray pole figures of YBCO on RABiTS in logarithmic scale for different thicknesses: (a) 0.19 μm, (b) 0.45 μm, (c) 1.6 μm, and (d) 3.0 μm. As YBCO thickness increases, significant degradation in cube texture is observed.

volume-percent cube texture, determined by quantifying the x-ray intensities from the background corrected pole figures, shows the percentage of the cube textured material dropped from 98.8% to 79.9% in a thickness range of 0.19–3 μm. This reduction in the percentage of cube texture is due to nucleation of 45° rotated grains as well as increased scatter in the films (in other words, a slightly increased fraction of randomly misoriented grains, which is not observed in the θ-2θ scans). The results are listed in Table II.

The next logical question is what would be the cause of the deterioration in the cube texture of thicker films on RABiTS. Several factors point to a change in surface temperature during the YBCO deposition as the reason. In an earlier study,[21] the substrate temperature was monitored by attaching the thermocouple wires on bare Ni strip at both ends of the RABiTS and was found to decrease with YBCO thickness as shown in Fig. 6. According to this data, if the temperature controller maintained a constant heater-block temperature, the substrate temperature would fall by as much as 30 °C during the 0.3-μm-thick YBCO deposition. A similar substrate temperature change during the YBCO deposition has been reported on single-crystal substrates as well by the means of infrared pyrometry.[22] This surface cooling has been explained by both a change in emissivity of the YBCO film and a change in thermal conductivity of the substrate and subsequent film layers.[8,23] As YBCO thickness increases (films get darker), an increase in film emissivity causes an increase in the rate of thermal radiation. This, coupled with decreasing thermal conductivity as the film grows, causes the surface to become cooler. Garcia-Moreno examined this process in detail.[23] This effect is even more apparent for STO due to its poorer thermal conductivity and greater thickness (about 10 times), and may account for the $a_{\perp}$ growth in thick YBCO films. To support this speculation, a systematic study on the effect of substrate temperature during the YBCO deposition is in progress.

As the films became thicker, different surface morphologies were found for YBCO films on each substrate. The SEM images of a series of YBCO films with different thickness on STO and on RABiTS are shown in Figs. 7(a) and 7(b) and Figs. 8(a)–8(d), respectively. On

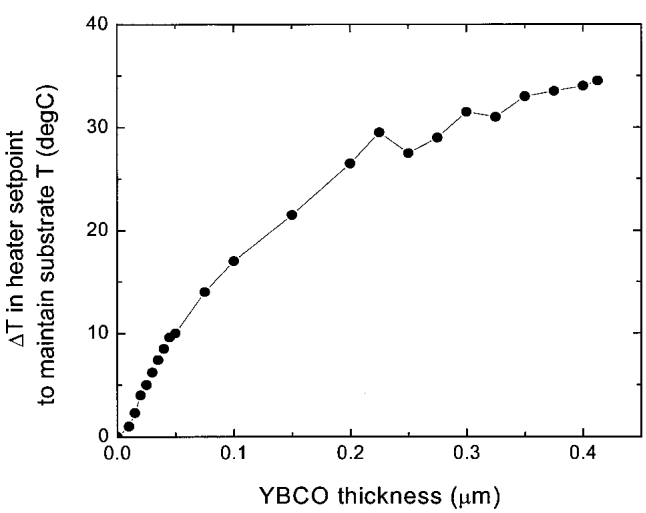

FIG. 6. Change of substrate temperature on RABiTS as a function of YBCO thickness. Surface temperature continuously decreases as YBCO thickness increases.

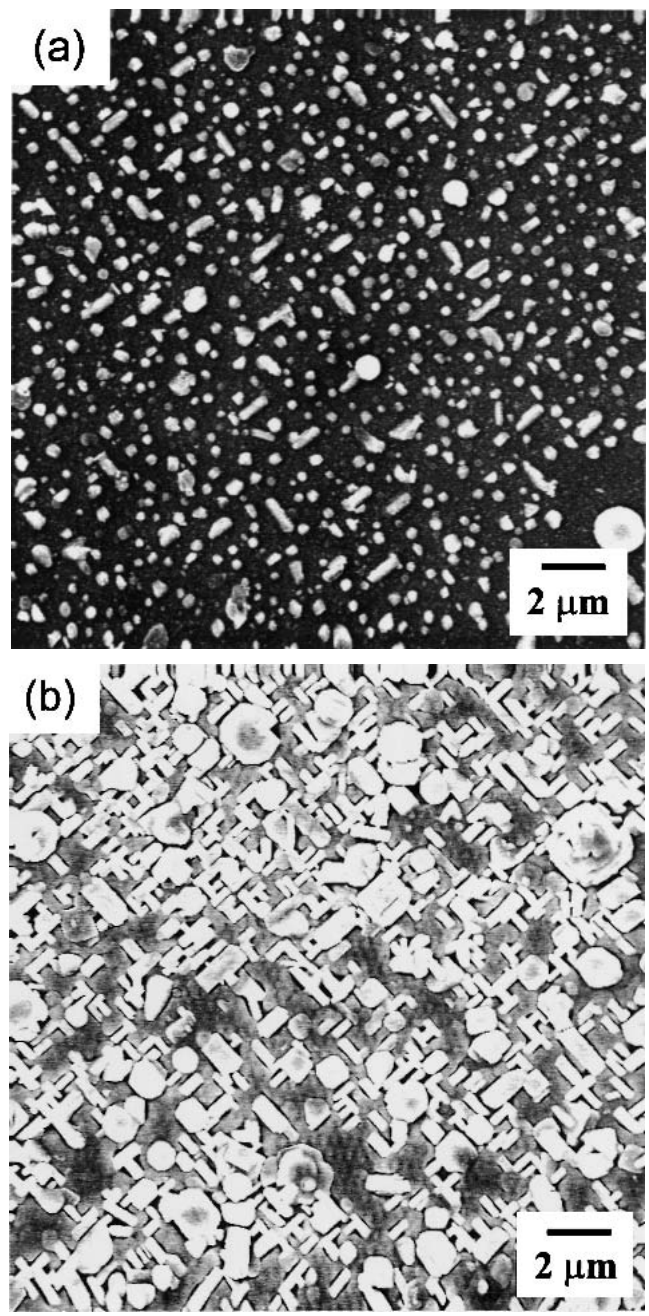

FIG. 7. SEM images of YBCO films on STO (a) 0.19 μm and (b) 1.8-μm-thick. Surface is covered by crisscrossed *a*-axis grains in the 1.8-μm-thick sample.

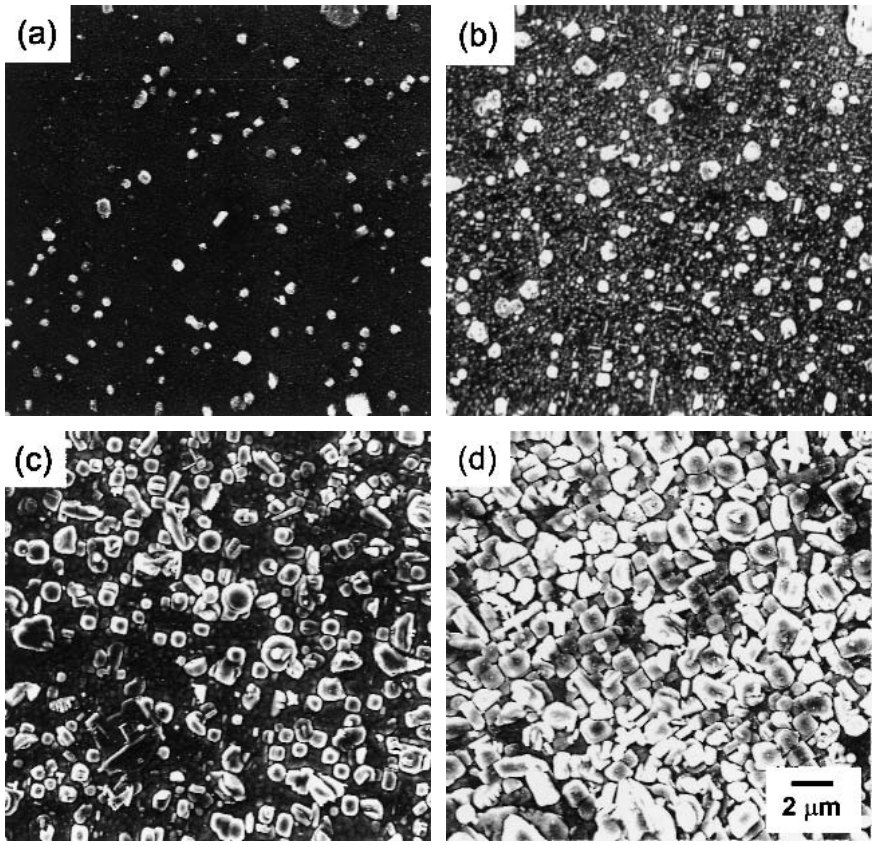

FIG. 8. SEM images of YBCO films on RABiTS (a) 0.19 μm, (b) 0.45μm, (c) 1.6 μm, and (d) 3 μm thick. Porosity and coarseness in surface morphology are developed as YBCO thickness increases.

both substrates, the surfaces were decorated by the second-phase particles including Cu-rich second-phase particles or $a_{\perp}$ grains as a feature of PLD YBCOs.[23,24] For thicker YBCO films on STO, clearly, a large fraction of $a_{\perp}$ grains consistent with the XRD χ-scan analysis, could be observed. The number fraction of second-phase particles seems to be smaller for the same thickness of YBCO film on RABiTS than on STO, which may be attributed to the different surface condition of the substrates. The 0.19-μm-thick YBCO on RABiTS exhibits a homogeneous, smooth, and dense surface morphology. As YBCO gets thicker, the number of particles increases and their average size gets bigger. The films also become more porous. For the 3.0-μm-thick YBCO sample, the surface is mostly covered with micron-sized, coarse, second-phase particles and pores. This rough surface morphology is similar to that of 6-μm-thick YBCO on metal substrates reported by Foltyn *et al.,*[12] who observed a clear distinction in morphology around 2 μm. Surprisingly, in our samples the surface coarseness starts as early as 0.45 μm, and it gradually develops with YBCO thickness. It has been found from magneto-optic imaging that pores and/or second-phase particles in the YBCO layer locally obstruct the superconducting current, causing an electromagnetic granularity and reducing J_c.[24] The same study also showed that in certain thick films, whenever second-phase particles were embedded inside the YBCO layer, YBCO did not grow on top of the second-phase particles for quite a distance into the film, resulting in cylindrical open pores in the YBCO films above the particle. Hence, it is likely that formation of coarse second-phase particles during PLD followed by extended pores on top of such particles reduces J_c substantially with increasing thickness.

Surface cooling may also have some effect on the second-phase distribution and size as well as porosity in the thick films. As pointed out by Ye and Nakamura,[26] low deposition temperatures can lead to cation disorder in thin films. This disorder, in turn, can produce a high density of defects in texture. These defects in YBCO are revealed in the XRD θ-2θ patterns. In particular, they showed that the ratio of the integrated intensity of the (006) peak to that of (005) is an indicator of cation disorder. The higher the ratio, the greater the disorder. An examination of the θ-2θ spectra of the films in this study reveals an increase in the ratio as thickness increases. Although unlikely, it is possible that the change in the ratio is due to oxygen deficiency in the YBCO. To confirm the presence of disorder, the films were examined using Raman spectroscopy. Gibson *et al.*[27] have shown

that the ratio of the forbidden 585 cm^{-1} Raman mode to the 340 cm^{-1} B_{1g} Raman mode is an indicator of the degree of disorder. For the present study, as the YBCO thickness increased the ratio Raman (585 cm^{-1}): Raman (340 cm^{-1}) also increased, indicating greater disorder. A transmission electron microscopy study of these samples is under way.

IV. SUMMARY

The thickness dependence of J_c for YBCO films on RABiTS and STO was studied. For YBCO films on both substrates, J_c versus thickness shows a similar functional dependence, even though the mechanisms for the J_c decrease with YBCO thickness are different for films on the two substrates. For YBCO films on STO, J_c degradation is dominated by the transition to $a_\perp$ growth and a broadening of the in-plane texture in thicker films. For YBCO films on RANTS, the formation of $a_\perp$ grains as well as broadening of the in-plane texture is not the dominant mechanism for the J_c degradation in thicker films. Instead, degradation in the overall percentage of cube texture of the YBCO film as well as the formation of significant porosity in thicker YBCO films appears to be the dominant mechanism.

Lastly, this study has shown that while the J_c of thick YBCO films on both RABiTS and STO decreases exponentially, the I_c of these films continues to increase. This implies that for applications involving conductors with higher I_c's, simply growing thicker YBCO films may work, provided that the J_c does not degrade.

ACKNOWLEDGMENTS

B.W. Kang is grateful to S.W. Lu for his help on RBS measurement. Research was sponsored by the United States Department of Energy, Office of Energy Efficiency and Renewable Energy, and Office of Power Technologies—Superconductivity Program. This research was performed at the Oak Ridge National Laboratory, managed by UT-Battelle, LLC for the United States Department of Energy under Contract No. DE-AC05-00OR22725. The authors (B.W. Kang and S. Sathyamurthy) are grateful to Oak Ridge Associated Universities for their support.

REFERENCES

1. X.D. Wu, S.R. Foltyn, P.N. Arendt, W.R. Blumenthal, I.H. Campbell, J.D. Cotton, J.Y. Coulter, W.L. Hults, M.P. Maley, H.F. Safar, and J.L. Smith, Appl. Phys. Lett. **67,** 2397 (1995).
2. A. Goyal, D.P. Norton, D.K. Christen, E.D. Specht, M. Paranthaman, D.M. Kroeger, J.D. Budai, Q. He, F.A. List, R. Feenstra, H.R. Kerchner, D.F. Lee, E. Harfield, P.M. Martin, J. Mathis, and C. Park, Appl. Supercon. **4,** 403 (1996).
3. A. Goyal, D.P. Norton, J.D. Budai, M. Paranthaman, E.D. Specht, B.M. Kroeger, D.K. Christen, A. He, B. Saffian, F.A. List, D.F. Lee, P.M. Martin, C.E. Klabunde, and V.K. Sikka, Appl. Phys. Lett. **69,** 1795 (1996).
4. Y. Ijima, M. Hosaka, N. Tanabe, N. Sadakata, T. Saito, O. Kohno, and K. Takeda, Appl. Supercond. **4,** 475 (1996).
5. A. Mogro-Campero, L.G. Turner, E.L. Hall, and N. Lewis, in *High-Temperature Superconductors: Fundamental Properties and Novel Materials Processing,* edited by D. Christen, J. Narayan, and L. Schneemeyer (Mater. Res. Soc. Symp. Proc. **169,** Pittsburgh, PA, 1990), p. 703.
6. F.E. Luborsky, R.F. Kwasnick, K. Borst, M.F. Garbauskas, E.L. Hall, and M.J. Curran, J. Appl. Phys. **64,** 6388 (1988).
7. S.R. Foltyn, P. Tiwari, R.C. Dye, M.Q. Le, and X.D. Wu, Appl. Phys. Lett. **63,** 1848 VVII (1993).
8. S. Sievers, F. Mattieis, H.U. Krebs, and H.C. Freyhardt, J. Appl. Phys. **78,** 5545 (1995).
9. S. Miura, K. Hashimoto, F. Wang, Y. Enomoto, and T. Morishita, Physica C **278,** 201 (1997).
10. A. Ignatiev, Q. Zhong, P.C. Chou, X. Zhang, J.R. Liu, and W.K. Chu, Appl. Phys. Lett. **70,** 1474 (1997).
11. V.F. Solovyov, H.J. Weisemann, L.J. Wu, M. Suenaga, and R. Feenstra, IEEE Trans. Appl. Supercond. **4,** 429 (1999).
12. S.R. Foltyn, Q.X. Jia, P.N. Arendt, L. Kinder, Y. Fan, and J.F. Smith, Appl. Phys. Lett. **75,** 3692 (1999).
13. M. Paranthaman, C. Park, X. Cui, A. Goyal, D.F. Lee, P.M. Martin, D.T. Verebelyi, D.P. Norton, D.K. Christen, and D.M. Kroeger, J. Mater. Res. **15,** 2647 (2000).
14. A. Goyal, D.P. Norton, J.D. Budai, M. Paranthaman, E.D. Specht, D.M. Kroeger, D.K. Christen, Q. He, B. Saffian, F.A. List, D.F. Lee, E. Harfield, P.M. Martin, C.E. Klabunde, E. Hatfield, and V.K. Sikka, Appl. Phys. Lett. **69,** 1795 (1996).
15. D.P. Norton, A. Goyal, J.D. Budai, D.K. Christen, D.M. Kroeger, E.D. Specht, Q. He, B. Saffian, M. Paranthaman, C.E. Klabunde, D.F. Lee, B.C. Sales, and F.A. List, Science **274,** 755 (1996).
16. F.A. List, A. Goyal, M. Paranthman, D.P. Norton, E.D. Specht, D.F. Lee, and D.M. Kroeger, Physica C **302,** 87 (1998).
17. M. Paranthaman, A. Goyal, F.A. List, E.D. Specht, D.F. Lee, P.M. Martin, Q. He, D.K. Christen, D.P. Norton, J.D. Budai, and D.M. Kroeger, Physica C **275,** 266 (1997).
18. Q. He, D.K. Christen, J.D. Budai, E.D. Specht, D.F. Lee, A. Goyal, D.P. Norton, M. Paranthaman, F.A. List, and D.M. Kroeger, Physica C **275,** 155 (1997).
19. A. Mogro-Campero, L.G. Turner, and E.L. Hall, J. Appl. Phys. **65,** 4951 (1989).
20. L. Luo, X.D. Wu, R.C. Dye, R.E. Muenchausen, S.R. Foltyn, Y. Coulter, and C.J. Maggiore, Appl. Phys. Lett. **59,** 2043 (1991).
21. J.E. Mathis, A. Goyal, F.A. List, P. Paranthaman, D.K. Christen, E.D. Specht, D.M. Kroeger, D.F. Lee, and P.M. Martin, Jpn. J. Appl. Phys. **37,** L1379 (1998).
22. T. Kiss, K. Enpuku, T. Matsumura, Y. Iriyama, T. Nakamura, and M. Takeo, IEICE Trans. Elec. **E79-C,** 1269 (1996).
23. F. Garcia Moreno, Temperature influences on the growth of HTS films (Diplomarbeit, University of Göttingen, Göttingen, Germany, 1995), chap. 4.
24. G. Koren, A. Gupta, R.J. Baseman, M.I. Lutwyche, and R.B. Laibowitz, Appl. Phys. Lett. **55,** 2450 (1989).
25. C-Y. Yang, A. Pashitski, A. Polyanskii, D.C. Larbalestier, S.E. Babcock, A. Goyal, F.A. List, M. Paranthaman, D.P. Norton, D.F. Lee, and D. M. Kroeger, Physica C **329,** 114 (2000).
26. J. Ye and K. Nakamura, Physica C **254,** 113 (1995).
27. G. Gibson, L.F. Cohen, R.G. Humphreys, and J.L. MacManus-Driscoll, Physica C **333,** 139 (2000).